



Numerical study of effects of vortex generators on heat transfer deterioration of supercritical water upward flow

Chika Eze ^a, Kin Wing Wong ^b, Tobias Gschnайдtn ^c, J. Cai ^d, Jiyun Zhao ^{a,*}

^a Department of Mechanical Engineering, City University of Hong Kong, Hong Kong

^b Department of Mechanical Engineering, ETH Zurich, Switzerland

^c Institute for Energy Systems, Technical University of Munich, Germany

^d School of Electric Power, South China University of Technology, Guangzhou, China



ARTICLE INFO

Article history:

Received 19 November 2018

Received in revised form 19 February 2019

Accepted 25 March 2019

Available online 29 March 2019

Keywords:

Supercritical water

Heat transfer deterioration

Heat transfer coefficient

Suppression

Delay

Vortex generator

ABSTRACT

The occurrence of heat transfer deterioration (HTD) in supercritical pressure boilers, where the wall temperature rises abruptly is an undesirable phenomenon that is limiting the design of new promising engineering applications. This may cause operational problems such as tube burnouts which could result in a catastrophic system failure. Understanding ways of eliminating HTD is of great importance for the design of safe and reliable supercritical pressure boilers. In this paper, vortex generators (VGs) are installed in circular and annular channels to investigate HTD phenomenon of supercritical water flowing upward at high heat flux and low mass flux using shear stress transport (SST) $k - \omega$ turbulence model in ANSYS-FLUENT. Results on wall temperature distribution for the smooth and enhanced channels are compared with available experimental data, and good agreements are obtained. The effects of VG's size, position, and number on HTD are investigated. The results indicate that VG's size slightly suppresses and delays HTD downstream of the VG, and there exists an optimum size beyond which HTD starts to aggravate. A strong effect of VGs on heat transfer coefficient (HTC) profiles is observed at locations where VGs are installed and at the downstream locations, with the normalized HTC showing that the wall temperature oscillates a couple of times before becoming stable once the flow returns to fully developed state. The VG's position has the most significant effect on HTD for any single VG. Increasing the number of VGs installed in-line at the start of the major peak baselines significantly suppresses and delays the peak. Mechanism analysis based on radial distributions of velocity and turbulent kinetic energy (TKE) at different axial positions of both channels shows that HTD suppression is caused by the weakening of the buoyancy effect due to increased TKE near the wall downstream of the VG, whereas the delay is caused by the boundary layer recovery effect due to flow redevelopment after being disrupted by the VG.

© 2019 Elsevier Ltd. All rights reserved.

1. Introduction

In the 1960s and 1970s, extensive research activities were carried out on heat transfer to fluids at supercritical pressures for the purpose of developing supercritical pressure fossil-fired power plants. In recent years, there has been a renewed interest in this field as a result of the new application of supercritical fluids, especially in nuclear industries. This is mainly due to the excellent heat transfer characteristics of supercritical fluids near the pseudo-critical point. For example, supercritical water reactors (SCWR), which is one of the most promising Generation IV nuclear reactor systems currently under development, is expected to yield thermal

efficiency of over 10% higher than currently-deployed light-water reactors (LWR). It is also expected to be more compact by eliminating the coolant recirculation pump, steam generators, steam separators, etc., which will further lower the operational and capital costs. In SCWR's fuel assembly, spacer grids or wire wrap spacers support the fuel pins in a vertical position and help to maintain a minimum spacing between fuel rods so that the entire length of the fuel channel can be adequately cooled. These spacers also influence the thermal and hydrodynamic performances of the fuel rods by acting like vortex generators (VGs)-disrupting the coolant flows and contributing to mixing between the subchannels. Therefore, understanding the effect of VGs on supercritical water heat transfer is important for the design of safe and reliable SCWR's fuel assembly.

The VGs are among the most popular actuators for the heat transfer enhancement of heat exchangers, whose main goal is to

* Corresponding author.

E-mail address: jiyuzhao@cityu.edu.hk (J. Zhao).

Nomenclature

A_{flow}	cross sectional area of flow [m^2]
C_p	specific heat at constant pressure, [$\text{kJ}/(\text{kg K})$]
C_μ	turbulence model's constant
D	diameter of the flow channel, [mm]
D_{in}, D_{out}	inner and outer diameter of the flow channel, [mm]
D_ω	cross-diffusion term
G	mass flux, [$\text{kg}/\text{m}^2 \text{s}$]
G_k, G_ω	production of turbulence kinetic energy and specific dissipation rate
g	gravitational acceleration, [m/s^2]
H	height of VG [mm]
H_b	bulk enthalpy [kJ/kg]
k	kinetic energy of turbulent fluctuations [m^2/s^2]
L	length of VG [mm]
$P, \Delta p$	pressure, [MPa] and pressure drop [Pa]
q	heat flux, [kW/m^2]
r	radial coordinate, [mm]
S	strain rate magnitude
T	temperature, [$^\circ\text{C}$]
T_b, T_w	bulk and wall temperature [$^\circ\text{C}$]
U, V	axial and radial velocity, [m/s]
x	axial coordinate, [mm]
y^+	dimensionless distance from the solid wall
Y_k, Y_ω	dissipation rate of k and ω

Non-Dimensional Numbers

$$\text{Pr, Re} \quad \text{Prandtl number} = \frac{\mu C_p}{k} \text{ and Reynolds number} = \frac{GD}{\mu}$$

Greek symbols

ε	turbulent dissipation rate [m^2/s^3]
μ	dynamic viscosity, [$\text{kg } /(\text{s m})$]
Φ	viscous dissipation
ω	specific turbulence dissipation rate [1/s]
ρ	density, [kg/m^3]
σ_t	turbulent Prandtl number = $\frac{\mu C_p}{k}$

Subscripts

b	bulk
e	effective
in	inner
out	outer
t	turbulent
w	wall

Acronyms and abbreviations

BR	Blockage Ratio
HTC	Heat Transfer Coefficient [$\text{kW}/\text{m}^2 \text{ } ^\circ\text{C}$]
HTD	Heat Transfer Deterioration
LWR	Light Water Reactor
rel. diff.	Relative difference
SCWR	Supercritical Water Reactor
SST	Shear Stress Transport
SWAMUP	Supercritical Water Multipurpose Test Loop
TKE	Turbulent Kinetic Energy
2D	Two Dimensional
VG	Vortex Generator

encourage/accommodate high heat fluxes within the bulk fluids. As a passive heat transfer element, the VG utilizes a special type of extended surface that mainly reenergizes the boundary layer of the fluid domain, and generates vortices parallel to the flow direction in order to achieve heat transfer enhancement [1–4]. The VGs interrupt the hydrodynamic and thermal boundary layers, inducing a recirculation zone or vortices flow behind it. The flow reattachment downstream of the VG gives rise to the washing up or down the channel walls leading to an increase in the heat transfer rate [5]. Intuitively, however, VGs may also be able to reduce the difference between the fluid and the wall temperatures for a given heat flux, thereby mitigating the heat transfer deterioration (HTD).

Apparently, vortices induced by VGs are classified into two categories-transverse vortices and longitudinal vortices. Transverse vortices and their generation influence the heat transfer mainly through flow disruption while longitudinal vortices and their generation have their impact on heat transfer rate by involving other heat transfer mechanisms such as enhanced turbulent intensity, induced swirl flow as well as flow mixing along the channel [6]. However, both categories of VGs can enhance heat transfer performance.

Many experiments and numerical simulations have been carried out to study the thermo-hydraulic behavior of VGs of various configurations but the majority of these studies are mainly for subcritical systems. Yoo et al. [7] performed an experimental investigation and found that flat tube heat exchanger with VGs can significantly enhance the heat transfer rate in comparison to conventional tube heat exchangers. Caliskan [8] investigated heat transfer enhancement in a channel with punched triangular and rectangular VGs and concluded that both VGs had significant enhancement effects on the heat transfer rate, in comparison to a smooth channel. Wang et al. [9] studied VGs effects on heat trans-

fer impingement using a pair of delta and rectangular winglet VGs. The results show that the rectangular winglet provides better heat transfer than the delta winglet due to the latter's weaker vortex flows. Zhou and Lu [10] performed thermal and flow characteristics of the plane and curved delta, trapezoidal and rectangular winglet VGs using the so-called synergy principle. The results show that although all VGs enhance thermo-hydraulic performance, the curved ones show better performance than plane ones. Song and Wang [11] investigated the effect of the number of VGs on heat transfer rate and reported that increased number of VGs need not always enhance the heat transfer rate.

Under supercritical pressure, the flow pattern is somewhat similar to the conventional single-phase flow in that liquid-vapor phase transition does not occur. However, near the pseudo-critical region supercritical fluids exhibit a unique drastic variation, leading to non-uniform heat transfer behavior over the fluid flow channel, and therefore causes the so-called HTD. Unexpected high values of wall temperature can be seen in some parts of the test section indicating the occurrence of HTD. The pressure vs. temperature diagram for water is shown in Fig. 1. There is a pseudo-critical line above the critical point, where the fluid does not undergo an actual phase transition but where the pseudo-critical temperature separates the fluid into liquid-like and gas-like states.

HTD phenomenon including its experimental observations and numerical analysis has been studied by several researchers since 1950s. Shitsman [13] carried out an experiment with water at supercritical pressure in the vertical circular channel at low mass flux and high heat flux, and first observed the HTD phenomenon in form of sharp and broad temperature peaks at some locations in the channel wall. Ornatskiy [14] investigated normal and deteriorated heat transfer in a vertical annular channel, and observed HTD visually as a red-hot spot at the upper section of the channel.

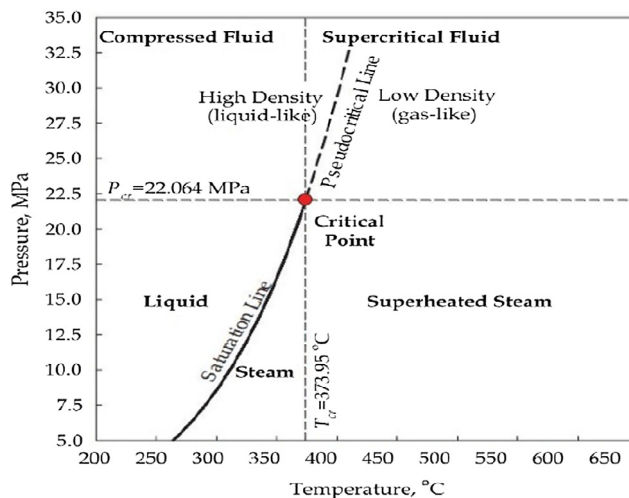


Fig. 1. Pressure vs. Temperature diagram for water [12].

The occurrence of HTD phenomenon has been attributed to the buoyancy force by Hall and Jackson [15–19]. This theory has been experimentally verified [20].

As for heat transfer enhancement at supercritical pressure, many studies focused on the effects of spacer grids in promoting heat transfer characteristics of annular flow channels. Gu et al. [21] experimentally studied effects of wire wrap spacers on supercritical heat transfer of water flowing in a 2×2 rod bundle. Bae et al. [22] performed an experimental study of heat transfer to supercritical carbon dioxide in a tube with wire wrap spacers. The result shows that the heat transfer was enhanced considerably due to the wire wraps. Zhu et al. [23] conducted a numerical investigation of grid spacer effect on heat transfer of supercritical water flows in a tight rod bundle. It was found that standard grid spacer design causes decreased heat transfer in a tight rod bundle. Recently, Yao et al. [24] conducted a numerical study of effects of spacer grids on heat transfer to supercritical R-134a and concluded that spacer end enthalpy has a remarkable influence on heat transfer enhancement. The authors also recommended the study of these effects on HTD. Wang et al. [25] studied the enhanced effect of spiral spacer on heat transfer of supercritical pressure water in vertical annular channels. The results reveal that these spacers have local and global heat transfer effects on supercritical water. Hu et al. [26] carried out experimental investigation of heat transfer of supercritical water in vertical annular channel equipped with spacers at the Supercritical Water Multipurpose Test Loop II (SWAMUP-II) facility in Shanghai Jiao Tong University. They concluded that spacers enhance heat transfer, and at certain location downstream of the spacers, heat transfer impairment is observed.

On the other hand, Guo, Yan, et al [27] reported that the size of the spacer grid can influence the fuel assembly's pressure loss, and the dynamic loads on grid spacers can adversely affect the geometrical structures especially during the Loss of Coolant Accident (LOCA) scenarios in nuclear reactors. However, in order to avoid spacer grid failure, the structural behaviour of fuel assemblies as well as their lateral strength and stiffness are usually taken into consideration during the design stage. [28]

Above mentioned studies indicate that most of the researches focus on heat transfer enhancement using VGs in subcritical channels and spacer grids, wire wrap or spiral spacers in supercritical annular channels. To the best of the authors' knowledge, no previous study has investigated the effect of VGs on HTD for supercritical fluids. Therefore, in support of the design of safe and reliable supercritical water heat exchanger systems, a detailed numerical

study has been carried out to explore the effects of VGs on the mitigation of HTD in circular and annular channels, taking into account the VGs size, position in the channel and number on wall temperature. In this work, we present a numerical simulation of HTD phenomena for supercritical water flowing upward at high heat flux and low mass flux in circular and annular channels with VG using ANSYS-FLUENT.

2. Geometry, boundary conditions, and governing equations.

2.1. Geometry description of the circular channel

The experimental data used is based on Shitsman's experiment [13], where subcritical water flows upward in an 8 mm inner diameter circular channel of length 2200 mm. The heated section is 2000 mm whereas the inlet and outlet extensions are 100 mm each. The inlet extension ensures that fully developed turbulent flow is achieved before the heated section, whereas the outlet extension ensures that there is no backflow at the outlet. Fig. 2 shows the schematic diagram of the circular channel with an inclusion of a VG in form of a protrusion, with Fig. 2(a) showing the full 3D of the channel including the VG. The interest of present study focuses on the suppression effect of rectangular VG on HTD based on Shitsman's experimental configuration. The choice of rectangular-shaped VG is based on simplicity for 2D axisymmetric modelling as shown in Fig. 2(b). Three cases were investigated as described in the table below. For all cases, the VG has the same length ($L = 2.0$ mm). In case 1, seven VGs of different heights (H) are installed at the same axial position ($x = 200$ mm) in the channel. In case 2, one VG ($H = 2$ mm and $L = 2$ mm) is separately installed at three different axial positions in the channel. For case 3, one, two and three VGs of the same size ($H = 2$ mm and $L = 2$ mm) are separately installed at three different axial positions ($x = 400$ mm, 650 mm and 850 mm) respectively. Table 1 summarises the various cases of the circular channel with VGs that were investigated.

2.2. Geometry description of the annular channel

In most SCWR concept designs, supercritical water flows in sub-channels between fuel rods. These sub-channels can be simplified to annular channels if the circumferential non-uniformity is not taken into consideration. In order to investigate the effect of VGs on heat transfer in supercritical water annular channel, the length of shitsman's channel is reduced so as to minimize computational cost. The geometric parameters consist of channel length 1200 mm with 100 mm inlet extension and 100 mm outlet extension. The inner diameter is 8 mm, the outer diameter is 11.314 mm and the equivalent diameter is 3.314 mm (see Table 2).

2.3. The VG configurations for the annular channel.

The rectangular-shaped VGs are directly installed around the inner wall of the annular channel as shown in Fig. 3. Since the length of the channel is reduced for this channel, the VG size is also reduced. Three cases were investigated. For all cases, the VG has the same length ($L = 0.2$ mm) and no VG is installed before $x = 100$ mm, so the fully developed turbulent flow is achieved before the flow encounters VGs. In case 1, four VGs of different heights are separately installed in the annular channel. In case 2, one VG ($H = 0.2$ mm and $L = 0.2$ mm) is separately installed at three different axial positions in the channel. In case 3, different numbers of VGs each of same size ($H = 0.2$ mm and $L = 0.2$ mm) are installed at three different axial positions.

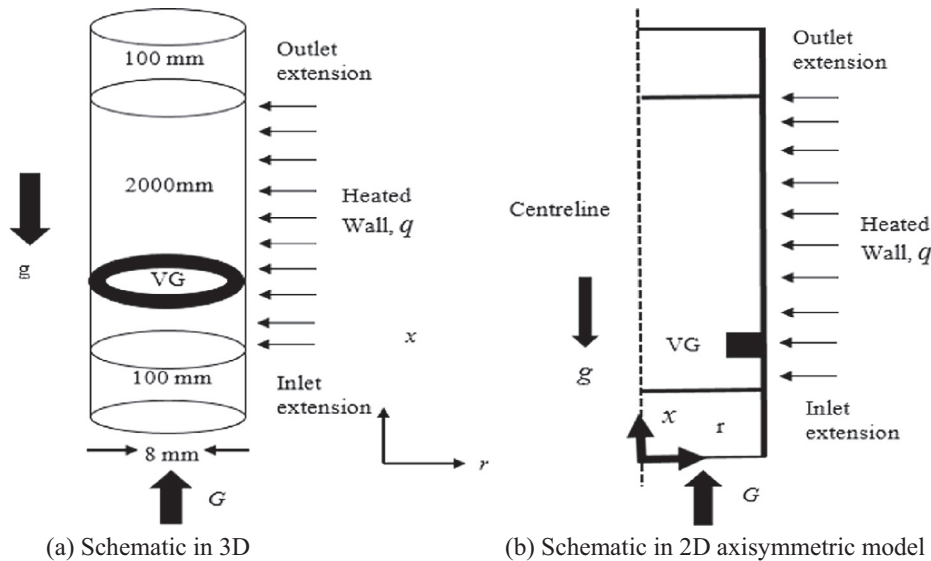


Fig. 2. Schematic of the circular channel, with an inclusion of a VG protrusion.

Table 1

The size, number and position of VGs in circular channel.

Cases	Geometry	Size (H (mm) by L (mm))	Position (mm)	Number	Effect
<i>1-Size (H (mm) by L (mm))</i>					
(i)	Circular	0.5 by 2.0	200	1	Size
(ii)	Circular	0.1 by 2.0	200	1	
(iii)	Circular	1.5 by 2.0	200	1	
(iv)	Circular	2.0 by 2.0	200	1	
(v)	Circular	2.5 by 2.0	200	1	
(vi)	Circular	3.0 by 2.0	200	1	
(vii)	Circular	3.5 by 2.0	200	1	
<i>2-Position (mm)</i>					
(i)	Circular	2.0 by 2.0	200	1	Position
(ii)	Circular	2.0 by 2.0	300	1	
(iii)	Circular	2.0 by 2.0	400	1	
<i>3-Number</i>					
(i)	Circular	2.0 by 2.0	400	1	Number (Downstream)
(ii)	Circular	2.0 by 2.0	400, 650	2	
(iii)	Circular	2.0 by 2.0	400, 650, 850	3	

Table 2

The size, number and position of VGs in annular channel.

Cases	Geometry	Size (H(mm) by L(mm))	Position (mm)	Number	Effect
<i>1-Size (H (mm) by L (mm))</i>					
(i)	Annular	0.1 by 0.2	150	1	Size
(ii)	Annular	0.2 by 0.2	150	1	
(iii)	Annular	0.3 by 0.2	150	1	
(iv)	Annular	0.4 by 0.2	150	1	
<i>2-Position (mm)</i>					
(i)	Annular	0.2 by 0.2	110	1	Position
(ii)	Annular	0.2 by 0.2	130	1	
(iii)	Annular	0.2 by 0.2	150	1	
<i>3-Number</i>					
(i)	Annular	0.2 by 0.2	150	1	Number (Downstream)
(ii)	Annular	0.2 by 0.2	150, 250	2	
(iii)	Annular	0.2 by 0.2	150, 250, 300	3	

2.4. Boundary and operating conditions

It is well known that there are two kinds of HTD phenomena that occur in supercritical systems: HTD at low mass flux which is caused by Buoyancy effect and HTD at high mass flux caused by acceleration effect. In this study, HTD occurring at low mass flux

is considered under the condition of high heat flux. For the circular channel simulation, both the geometry and operating conditions are based on Shitsman's experimental results [13]. Hence, the operating pressure is 25.3 MPa and the water temperature at the inlet of the computational domain is 324 °C. The pseudo-critical temperature at 25.3 MPa is 386 °C. The heat flux is 384.8 kW/m²

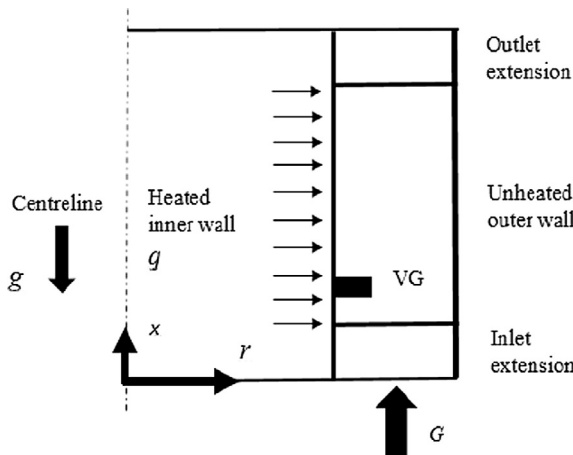


Fig. 3. Schematic of the annular channel, with an inclusion of a VG protrusion in 2D axisymmetric model.

and the mass flux is $449 \text{ kg/m}^2 \text{ s}$. For the annular channel, since the experiments of HTD in annular channel at low mass flux are not available in the open literature, the conditions of Shitsman's experiment in circular channel were slightly modified and considered in annular channel. Firstly, in order to reveal clearly the occurrence of HTD for this channel, slightly higher heat flux, lower mass flux and lower operating pressure of 400 kW/m^2 , $350 \text{ kg/m}^2 \text{ s}$ and 25 MPa respectively were supplied. Secondly, the heated length of this channel is halved to minimise the computational time, and the inlet temperature is slightly increased to 360°C to shift the position of HTD occurrence towards the channel's inlet. For both channels, the inlet boundary condition is mass flow inlet, and the outlet boundary condition is pressure outlet. No-slip boundary conditions are adopted at the channel walls and the VGs. The turbulent intensity and turbulent viscosity ratio at inlet are set as 5% and 10% respectively. Uniform heat fluxes are applied at the wall and water flows upwards under gravity (g).

2.5. Governing equations and turbulence models

A variety of turbulence models are provided in ANSYS FLUENT, and all models meet the following fundamental governing equations of conservation of mass (1), momentum ((2) and (3)) and energy (4) for 2-dimensional (2D) axisymmetric model in cylindrical coordinates as:

Continuity:

$$\frac{1}{r} \left\{ \frac{\partial}{\partial x} (r \rho U) + \frac{\partial}{\partial r} (r \rho V) \right\} = 0 \quad (1)$$

Momentum:

The momentum conservation equation has forms of the following differential equations- in both radial and axial coordinates:

Axial Momentum:

$$\begin{aligned} \frac{1}{r} \left\{ \frac{\partial}{\partial x} (r \rho U^2) + \frac{\partial}{\partial r} (r \rho VU) \right\} &= - \frac{\partial p}{\partial x} + \rho g \\ &+ \frac{1}{r} \left\{ 2 \frac{\partial}{\partial x} \left(r \mu_e \left(\frac{\partial U}{\partial x} \right) \right) + \frac{\partial}{\partial r} \left(r \mu_e \left(\frac{\partial U}{\partial r} + \frac{\partial V}{\partial x} \right) \right) \right\} \end{aligned} \quad (2)$$

Radial Momentum:

$$\begin{aligned} \frac{1}{r} \left\{ \frac{\partial}{\partial x} (r \rho UV) + \frac{\partial}{\partial r} (r \rho V^2) \right\} \\ = - \frac{\partial p}{\partial r} + \frac{1}{r} \left\{ \frac{\partial}{\partial x} \left(r \mu_e \left(\frac{\partial V}{\partial x} + \frac{\partial U}{\partial r} \right) \right) + 2 \frac{\partial}{\partial r} \left(r \mu_e \left(\frac{\partial V}{\partial r} \right) \right) \right\} - 2 \frac{\mu_e V}{r^2} \end{aligned} \quad (3)$$

where U is the velocity in the x -direction, V is the velocity in the r -direction, ρ is the density. And x and r denote the axial and radial coordinates respectively, μ_e is the effective viscosity defined by $\mu_e = \mu + \mu_t$ and μ is the fluid viscosity while μ_t is the turbulent viscosity.

Energy:

$$\begin{aligned} \frac{1}{r} \left\{ \frac{\partial}{\partial x} (r \rho Uh) + \frac{\partial}{\partial r} (r \rho Vh) \right\} \\ = \frac{1}{r} \left\{ \frac{\partial}{\partial x} \left(r \left(\frac{\mu}{Pr} + \frac{\mu_t}{\sigma_t} \right) \frac{\partial h}{\partial x} \right) + \frac{\partial}{\partial r} \left(r \left(\frac{\mu}{Pr} + \frac{\mu_t}{\sigma_t} \right) \frac{\partial h}{\partial r} \right) \right\} \end{aligned} \quad (4)$$

Also, h is the enthalpy, Pr is molecular Prandtl number and σ_t is the turbulent Prandtl number. The constant 0.9 is used for σ_t in the simulation.

2.6. Turbulence model

Turbulence model plays an important role in numerical analysis. Generally, ANSYS FLUENT provides many choices of turbulent models such as standard $k-\epsilon$ model, realizable $k-\epsilon$ model, RNG $k-\epsilon$ model, LES model as well as shear stress transport (SST) $k-\omega$ turbulence model. The SST $k-\omega$ turbulence model was chosen for this study.

2.6.1. SST $k-\omega$ turbulent model

In the transport equations for Shear Stress Transport (SST) $k-\omega$ models, the turbulence kinetic energy, k is obtained by solving the following equations:

$$\begin{aligned} \frac{\partial}{\partial t} (\rho k) + \frac{\partial}{\partial x} (\rho k U) + \frac{\partial}{\partial r} (\rho k V) \\ = \frac{\partial}{\partial x} \left[\left(\mu + \frac{\mu_t}{\sigma_k} \right) \frac{\partial k}{\partial x} \right] + \frac{\partial}{\partial r} \left[\left(\mu + \frac{\mu_t}{\sigma_k} \right) \frac{\partial k}{\partial r} \right] + G_k - Y_k \end{aligned} \quad (5)$$

Whereas the specific dissipation rate, ω is obtained by solving equation below:

$$\begin{aligned} \frac{\partial}{\partial t} (\rho \omega) + \frac{\partial}{\partial x} (\rho \omega U) + \frac{\partial}{\partial r} (\rho \omega V) \\ = \frac{\partial}{\partial x} \left[\left(\mu + \frac{\mu_t}{\sigma_\omega} \right) \frac{\partial \omega}{\partial x} \right] + \frac{\partial}{\partial r} \left[\left(\mu + \frac{\mu_t}{\sigma_\omega} \right) \frac{\partial \omega}{\partial r} \right] + G_\omega - Y_\omega + D_\omega \end{aligned} \quad (6)$$

where G_k is the production of turbulence kinetic energy, k and G_ω is the generation of specific dissipation rate, ω . The term Y_k denotes the dissipation rate of k , Y_ω is the dissipation rate of ω , and D_ω is the cross-diffusion term. μ_t is the turbulent viscosity for SST $k-\omega$, which is also given as:

$$\mu_t = \frac{\rho k}{\omega} \frac{1}{\max(\frac{1}{\alpha^*} + \frac{SF_2}{\alpha_1 \omega})} \quad (7)$$

where S denotes the strain rate magnitude, α^* (equal unity for high Reynolds no) is a coefficient included in order to describe the non-linear transition of flow regime from laminar flow into turbulent flow, and F_2 is given by:

$$F_2 = \tanh(\Phi_2^2) \quad (8)$$

And

$$\Phi = \max \left[2 \frac{\sqrt{k}}{0.09 \omega y}, \frac{500 u}{\rho y^2 \omega} \right] \quad (9)$$

where y denotes the distance to the next surface.

Literally, SST $k-\omega$ model was developed by the combination of $k-\omega$ and $k-\epsilon$ models. The use of $k-\omega$ formulation in the inner

parts of the boundary layer makes the model directly usable all the way down to the wall through the viscous sub-layer in the near wall region. Whereas the use of $k - \varepsilon$ in the free stream in the far field of the flow avoids the common $k - \omega$ problem that the model is too sensitive to the inlet free-stream turbulence properties. Their combination is done by converting $k - \varepsilon$ model into $k - \omega$ with the use of multiplications results from both models by blending function, and adding them together. Hence, the blending function is unity in near-wall region in so that the $k - \omega$ model is used and zero away from the surface such that $k - \varepsilon$ model is used. It can be concluded that the SST $k - \omega$ combines $k - \omega$ and $k - \varepsilon$ in order to provide accurate results both at near wall and in the free stream. Moreover, this turbulence model has been tested and recommended for modeling the heat transfer to supercritical water, including the deteriorated region by researchers such as Palko, Jaromin, and Cheng et al [29–31].

2.7. Calculated parameters

In some cases, the analysis is based on calculated parameters, such as bulk enthalpies and heat transfer coefficient.

2.7.1. Bulk enthalpy

The bulk enthalpies at different axial positions of the heated section are calculated by the following heat balance equation below:

$$h_b = h_{in} + \frac{q\pi Dx}{GA_{flow}} \quad (10)$$

where h_{in} is the bulk enthalpy at the inlet of heated section, evaluated with the inlet pressure and inlet fluid temperature from NIST REFPROP Database [32], x is the axial distance at any location from the start of the heated length, G is the mass flux, q is the heat flux, D is the tube diameter and A_{flow} is the cross sectional area of flow.

2.7.2. Heat transfer coefficient

For practical engineering application, heat transfer coefficient is much more useful than wall temperature. The heat transfer coefficient is defined as:

$$HTC = \frac{q}{(T_w - T_b)} \quad (11)$$

where q is the heat flux, T_w is the local wall temperature, T_b is the local bulk-fluid temperature, evaluated according to bulk pressure and enthalpy using the NIST REFPROP [32].

3. Numerical simulation

The commercial software ANSYS Fluent 17.0 is used for the CFD simulations. The computational domain is discretized by a structured mesh generated using the commercial software ICEM. A typical structured grid system used in the generation of meshes in ICEM for the smooth channel (a) and channel with VG (b) is shown in Fig. 4. Generally, ANSYS FLUENT provides many choices of turbulent models such as standard $k - \varepsilon$ model, realizable $k - \varepsilon$ model, RNG $k - \varepsilon$ model, LES model as well as shear stress transport (SST) $k - \omega$ turbulence model. The $k - \omega$ SST turbulence model has been tested and recommended for modeling the heat transfer to supercritical water, including the deteriorated region by Palko, Jaromin, and Cheng et al. [29–31]. Fluent is linked to NIST Standard Reference Database 23, version 9.1 software [32] for retrieving thermo-physical properties of the supercritical water. The SIMPLE scheme was used to couple the pressure and velocity in the momentum equation. The continuity, momentum, and energy

equations were performed by the second-order upwind scheme. The convergence criterion for the normalized residual of individual governing equations was set to be less than 1.0×10^{-6} to minimize the linearization error. During numerical simulation process, the inlet boundary condition is mass flow inlet, and the outlet boundary condition is pressure outlet. No-slip boundary conditions are adopted at the channel walls and the VGs. The inlet and outlet extensions of the channels are considered as adiabatic.

3.1. Circular channel simulation

3.1.1. Grid independent test

Mesh sensitivity analysis is an important issue for a good performance of numerical simulation. Since y^+ can be defined as the non-dimensional distance between the wall and the first computational node, the first node was placed 0.001 mm from the wall so that, y^+ of the first element near the wall is less than 1 as recommended by Cheng and Yang [33,34]. The main reason is that the $k - \omega$ SST turbulent model does not use any wall functions. For the smooth channel, the total element of the first grid is 51,000. Grid refinement was carried out based on the method proposed by Celik et al. [35] which recommends that the grid refinement factor (r) should be greater than 1.3. Hence, $r = 1.4$ was chosen to generate three more meshes with about 40% element count increment. The number of elements of these meshes are 71,000, 99,000 and 138,600 respectively as shown in Fig. 5(a). The results indicate that the wall temperature no longer changes when the grid number is greater than 99,000. Hence bearing in mind the computational time, the grid system with 99,000 elements is accurate enough for the simulations. For the channel with VGs, further grid refinement was carried out and it was found that channel with VG requires slightly more grid numbers to attain convergence and capture its effects. The VG of height 2 mm is arbitrarily selected for grid convergence test. The results indicate that the wall temperature no longer changes significantly when the grid number for the channel with VG is greater than 100,450 as shown in Fig. 5(b). And since all VGs have the same length of 2 mm, equal grid numbers are used for all calculations in channels with VGs. These tests demonstrate that the grid systems with 99,000 elements and 100,450 elements are accurate enough for the simulations of the smooth channel and channel with VG respectively.

4. Circular channel results and discussions

4.1. Validation of smooth channel

In order to validate the accuracy of the numerical simulation, comparison with the experimental data is necessary. The simulation results of wall temperature distribution along the axial direction are compared to those of the Shitsman's water experiment [13] as shown in Fig. 6. Although the analysis does not fit perfectly well with the experimental wall temperatures, it captured appropriately the general trends of the experimental results. The results of the present study show that there are two wall temperature peaks occurring in the channel. The first peak called the major HTD is sharp while the second called the minor HTD is broadened. The wall temperature peaks of the major HTD for both results match almost perfectly (the difference is only up to 6 °C) even though their positions do not fit very well. In fact, previous studies [36,37] have also confirmed that CFD simulations don't perfectly fit with experimental results, rather they tend to either under or over-predict the wall temperature and that the locations of the predicted wall temperature peaks usually shift downstream. Thus, this shows that the simulation data for wall temperature are in good agreement with the experimental data measurement.

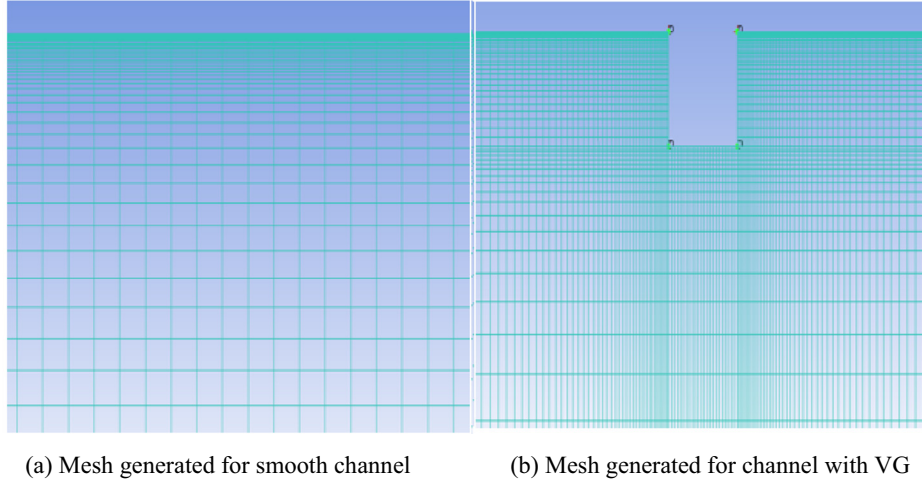


Fig. 4. Generation of Meshes in ICEM CFD for a circular channel.

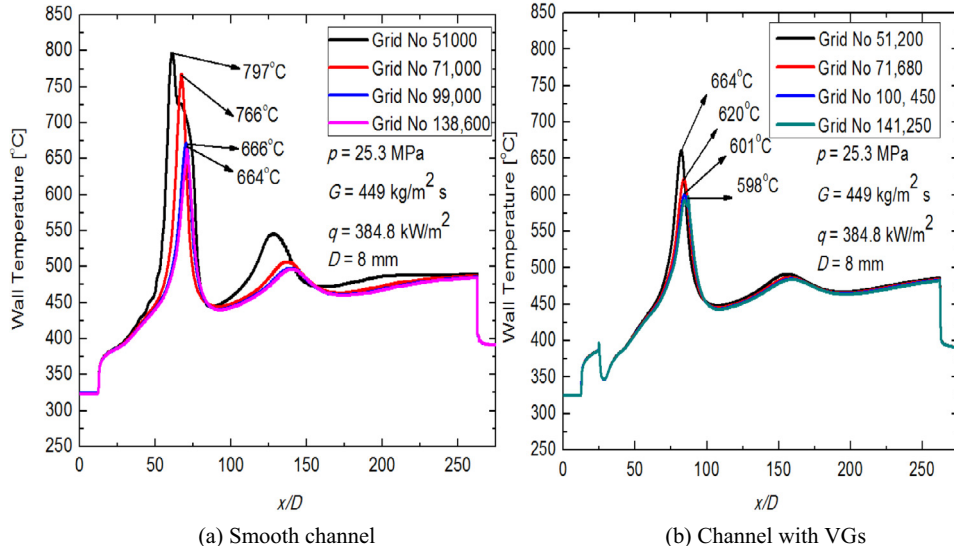


Fig. 5. Circular channel grid independent tests.

4.2. Validation of the enhanced channel

There are no existing experimental data to validate the enhanced channels for the current models where VGs are installed as protrusion to heat transfer surfaces in circular and annular channels of water flowing upward at supercritical pressure. However, there exists experimental data by Hu et al. [26] on heat transfer enhancement of supercritical water in an annular channel using spacer grids, which was carried out at the SWAMUP-II facility in Shanghai Jiao Tong University. Fig. 7 shows the wall temperature distribution for numerical and experimental results for the channel enhanced with spacer grid. At the location of the spacers (spacer1 and spacer2 have blockage ratios (BR) of 0.2 and 0.3 respectively), the wall temperature decreases significantly showing that spacer-induced heat transfer enhancement has been observed. The result also shows that variation trend of the simulated result matches well with the experimental result. Hence, it is considered that the current model is capable to simulate VG's effect on flow and heat transfer of the supercritical water.

4.3. Effect of VG's size on HTD

Fig. 8 illustrates the heat performance effect of different sizes (heights) of VGs. Fig. 8(a) shows the VG's size effects on wall temperature, revealing suppression of HTD starting from a height of 0.5 mm up to 2 mm with the major temperature peak decrease of 65 °C for a VG of height 2 mm. Fig. 8(b) shows the positions of major temperature peaks (including the overlapping peaks) at different axial VG positions, revealing that the VG's size slightly delays the occurrence of HTD. Beyond the VG of height 2 mm, both the size of major temperature peaks and the positions where they occur are nearly unchanged. This suggests that there exists an optimum size of VGs which can have a significant mitigation effect on the HTD. The heat transfer coefficient (HTC) and its normalised form are presented in Fig. 8(c) and Fig. 8(d) respectively. It is seen that the local heat transfer performances are quite distinguishing, and at the position where the VGs are installed, the local heat transfer is greatly enhanced. Downstream of the VG, HTC shows a couple of oscillations which become stable only when HTC

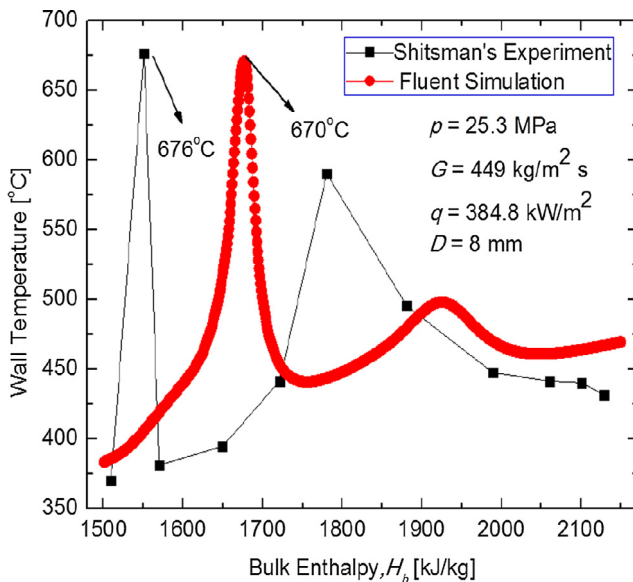


Fig. 6. Comparison of results from CFD and experimental wall temperature distribution in a smooth channel [13].

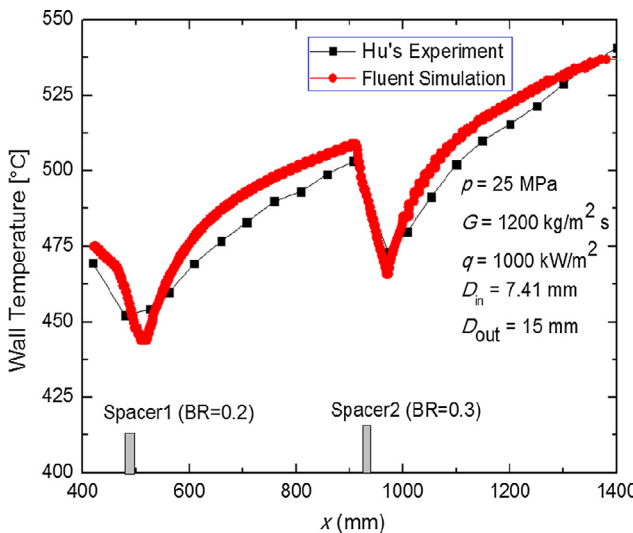


Fig. 7. Comparison of results from CFD and experimental wall temperature distribution in an enhanced channel [26].

reaches that of the fully developed condition. These oscillations are due to the occurrence of the suppressed and delayed HTD and subsequent wall temperature recovery at different axial locations of the channels with VG. Given that VG of size 2 mm by 2 mm has the best performance on suppressing the wall temperature peaks, it was selected to examine wall temperatures at various positions along the channel and for various number of VGs in the channel.

To further analyze why the heat transfer performance is not further improved after the height is increased larger than 2 mm, the plots of streamline velocity were considered for VGs of different sizes as shown in Fig. 9. It can be seen that for all VG sizes considered, the flow of water downstream experiences flow separation, backflow, and reattachment, generating vortices at the trailing edge of the VGs. Obviously, the strength and extent of these effects are significantly increased with the increase of VG height (i.e. size). Furthermore, near the position where the VGs are installed, the velocity increases very dramatically with the increase of VG size

because, from the law of continuity, the bigger VG must generate higher velocity due to the blockage effect. This eventually weakens the buoyancy effect on the turbulent heat transfer. Beyond a height of 2 mm (i.e. size 2 mm by 2 mm), the pressure drop starts to become very high as shown in Table 3. Since HTD tends to weaken and worsen with a pressure rise and drop respectively near the pseudo-critical pressure [38], the authors believe that the pressure drop effect is the reason behind HTD aggravation beyond the optimal size.

4.4. Effect of VG's position on HTD

Fig. 10 shows the heat performance effect of placing VG at different axial positions along the channel. Wall temperature distributions in the channel at different axial VG positions are compared with the channel without VGs and the results reveal that when VG is placed close to the point where major temperature peak normally occurs for a smooth channel, significant suppression, and delay of HTD is observed, whereas when it is placed further away before this position this effect greatly reduces. In order to avoid placing a VG at points where HTD already occurs, the start of the major peak baseline ($x = 400 \text{ mm}$) is taken to be the highest position where VG is placed. It is worth noting that the start of the major peak baseline is a selected point before the axial position corresponding to the pseudo-critical temperature. The greatest suppression and delay of HTDs are observed when VGs are placed within this position. At this position, the major temperature peak drops by about 101 °C.

4.5. Effect of VG's number on HTD

Fig. 11 presents the effects on wall temperature when different number of VGs are installed in a circular channel. The HTD suppression and delay tend to increase significantly with increase in the number of VGs. The channel with three VGs provides the highest value of suppression and delay (at the expense of higher pressure drop penalty) with a broadened major temperature peak, while that with one VG yields the lowest. In fact, the greater the size and number of VGs in the channel, the greater is the pressure drop as shown in Table 3. This indicates that increasing the number of VGs and size (beyond the so-called optimal size) are not necessarily advantageous in the design of supercritical heat exchanger systems. Hence, among all cases investigated, a single optimal sized VG installed at the start of the major peak baselines should be used to obtain highest suppression and delay of HTD and therefore should be used in designing safer SCWR's fuel assembly.

4.6. Mechanisms of VG's mitigation effects on HTD

To explain this phenomenon, a circular channel with VG of height 2 mm placed at the axial position of 200 mm was arbitrarily selected and plotted with the smooth channel. Fig. 12 is divided into three Phases at different axial positions. Phase 1 denotes selected positions before the VG, Phase 2 denotes downstream selected positions immediately after the VG and Phase 3 is the selected downstream positions further away from the VG. In addition, Fig. 13 shows the velocity streamlines of both channels in order to illustrate the channels' velocity flow structures across the entire channels.

Fig. 14 shows the radial distributions of velocity and TKE at different axial positions for Phase 1. Fig. 14(a) shows that the velocity profile is fully developed for both channels in this phase. Due to the buoyancy effect, mean velocity profile appears to flatten around radial positions ($r = 0.5R$) for both channels, leading to a decrease in TKE as seen in Fig. 13(b) below. This eventual reduction of TKE impairs the turbulent diffusion leading to HTD.

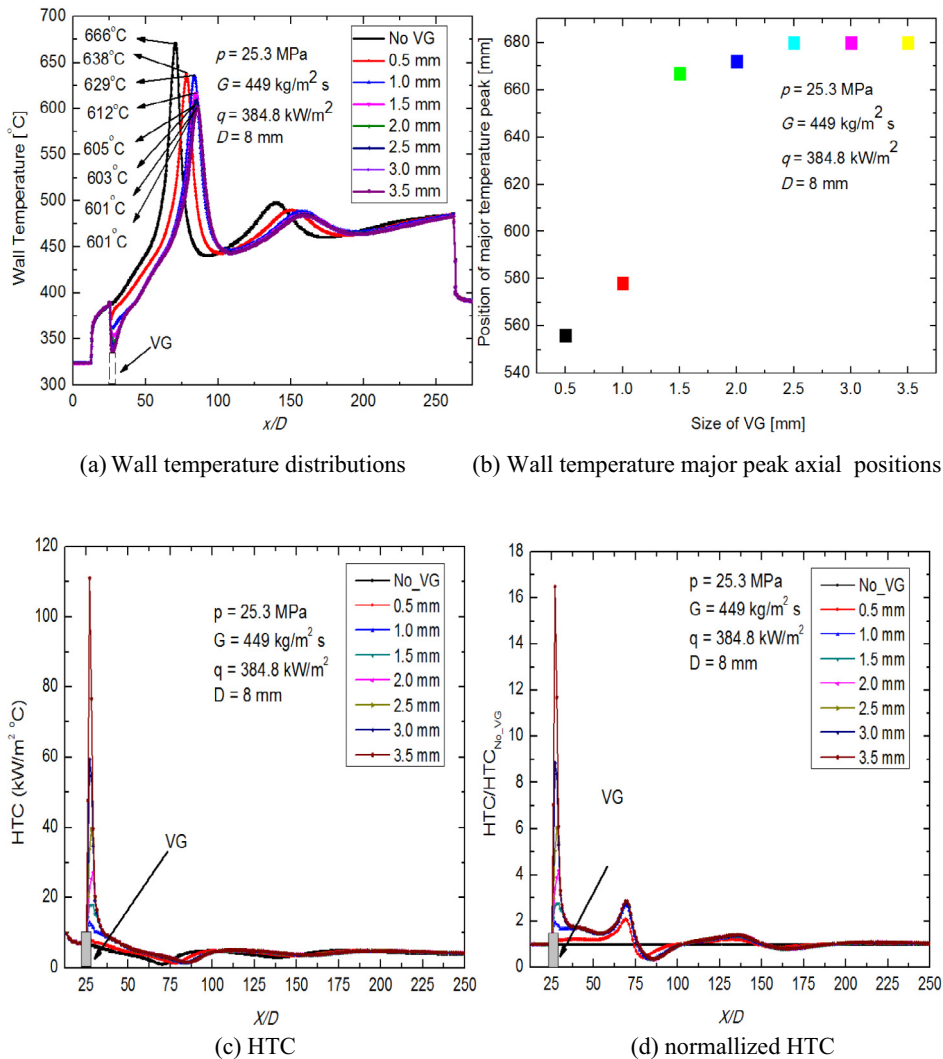


Fig. 8. Effects of VG's size on HTD in a circular channel.

Fig. 15 illustrates the radial distributions of velocity and TKE at different axial positions for Phase 2. The velocity near the wall for the channel with VG is slightly lower than that of the fully developed channel without VG because the fluid near the wall is separated by the VGs in the near-wall region at this Phase. Thus, producing a small region of stagnation zone as revealed in the velocity streamline (**Fig. 13(b)**). Away from the wall towards the centreline, the velocity for the channel with VG increases dramatically and becomes higher than that of the fully developed channel without VG. This is caused by the strong secondary flow in the radial direction as a result of sudden flow area reduction around VGs that promotes turbulence production. The TKE peak indicates that the TKE at this location was destructed by the VGs effect resulting in the sharp temperature drop near the positions where VGs are installed. For the smooth channel, the velocity profile in this phase remains fully developed. However, TKE slightly increases, which causes the gradual recovery of the wall temperature.

Fig. 16 shows the radial distributions of velocity and TKE at different axial positions for Phase 3. For the channel with VG, as the flow develops, the velocity field starts to re-establish with a decrease of velocity near the wall until the flow becomes fully developed attaining the same trend and values as the smooth

channel. However, the values of the TKE when the flow has fully redeveloped is slightly higher near the wall when compared with those of smooth channel. This might cause a reduction of the buoyancy effect. However, even though the wall temperature increases drastically again beyond this region and deteriorates again, the temperature peak is lower and delayed compared with that of the smooth channel.

4.7. Further investigation of effects of VG on buoyancy flow

In what follows, VG's effect on the buoyancy is further presented in **Fig. 17**. The supercritical water flows in smooth channel and channel with VG is simulated and the wall temperature distribution is compared under the same operating conditions with and without gravity as shown in **Fig. 17** (a). Owing to the buoyancy effect, HTD occurs in the vicinity of pseudo-critical temperature for both channels under gravity, although the wall temperature peaks are greatly suppressed for the channel with VG, indicating that the heat transfer experienced a less severe deterioration under this condition. For the condition of no gravity, HTD completely disappears for both channels and apart from the region where VG is installed, the wall temperature distribution is almost completely indistinguishable in both channels.

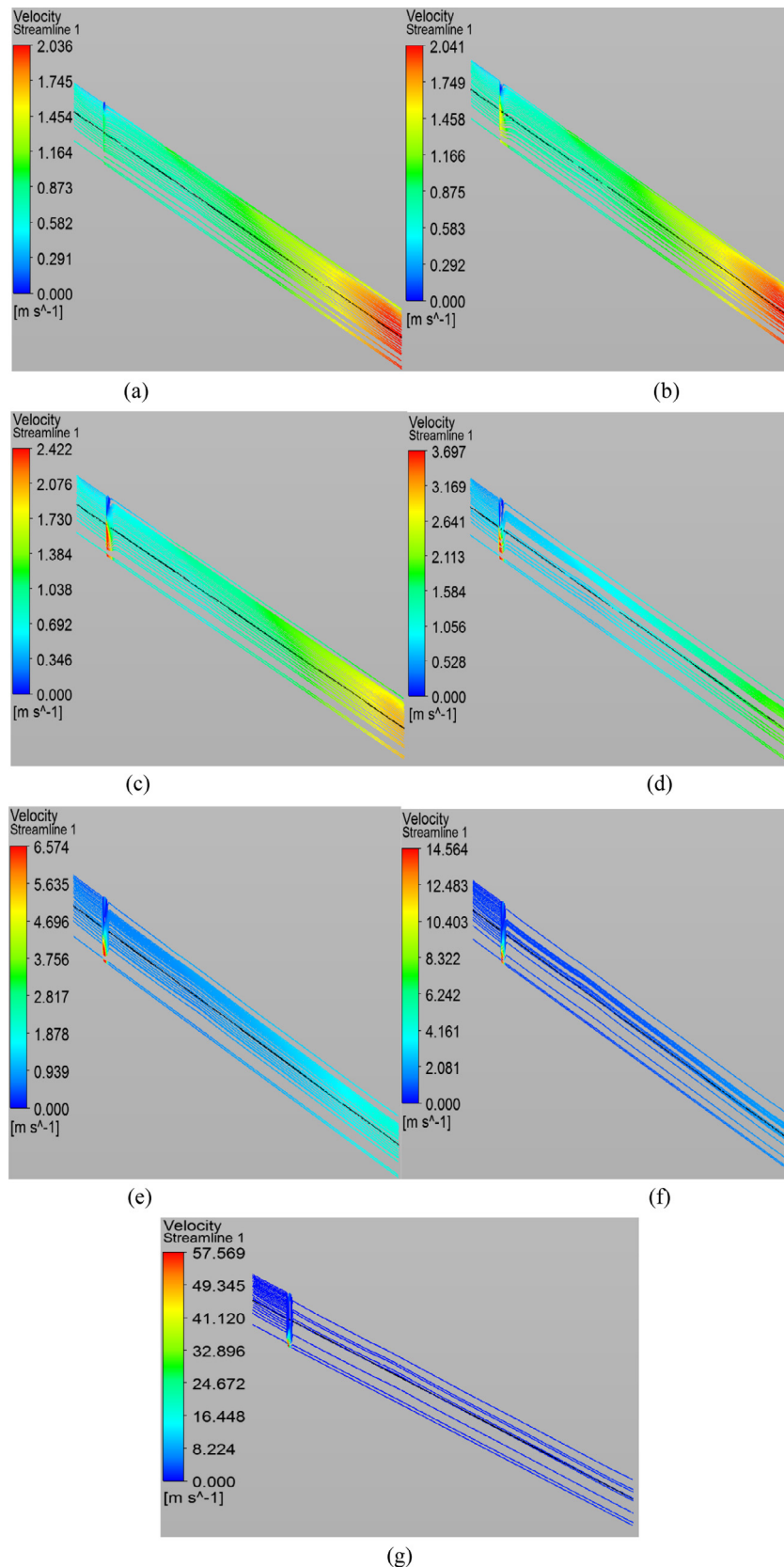


Fig. 9. Comparison of velocity streamlines for VGs of different sizes (H by L): (a) VG of size 0.5 mm by 2 mm, (b) VG of size 1 mm by 2 mm, (c) VG of size 1.5 mm by 2 mm, (d) VG of size 2 mm by 2 mm, (e) VG of size 2.5 mm by 2 mm, (f) VG of size 3 mm by 2 mm, (g) VG of size 3.5 mm by 2 mm.

Table 3

Pressure drop for Circular Channel with VGs.

Case	Total Pressure drop, Δp (Pa)	Δp rel. diff., %
Smooth channel	1473	reference case
1-Size (H (mm) by L (mm))		
(i)	1484	0.8
(ii)	1492	1.3
(iii)	1505	2.2
(iv)	1580	7.3
(v)	2362	60.4
(vi)	3763	155.5
(vii)	23,967	1527.1
2-Position (mm)		
(i)	1580	7.3
(ii)	1595	8.3
(iii)	1608	9.2
3-Number		
(i)	1608	9.2
(ii)	1788	21.4
(iii)	1819	23.5

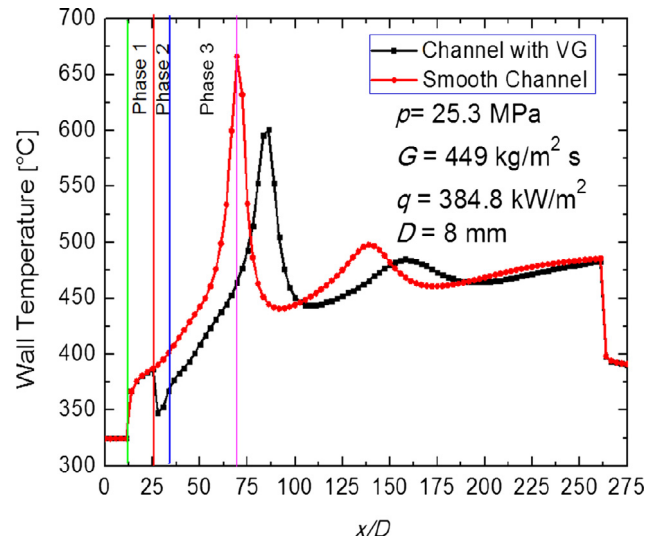
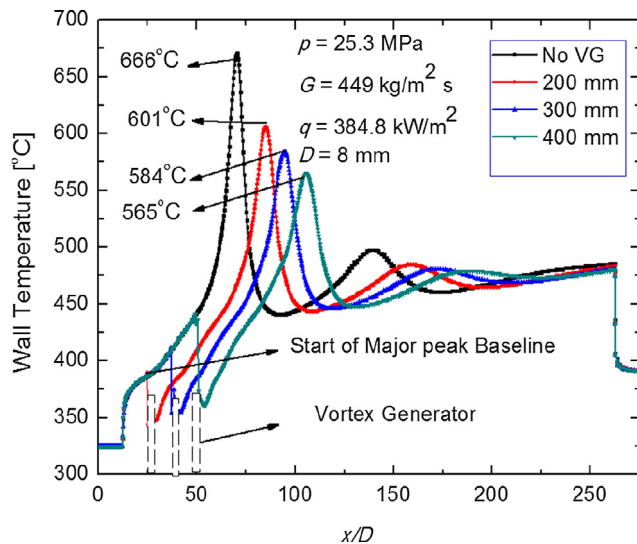
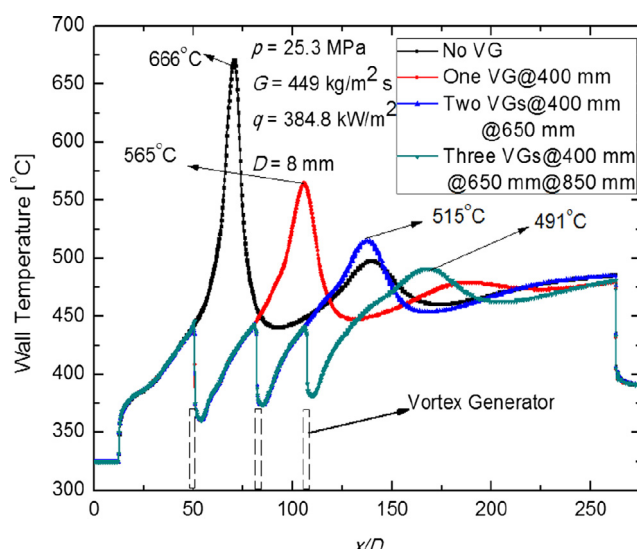
**Fig. 12.** Three Phases of the circular channel wall temperature distribution.**Fig. 10.** Effects of Positions of VG on HTD in a circular channel.**Fig. 11.** Effects of different number of VGs on HTD in a circular channel.

Fig. 17(b) shows the calculated results of the supercritical water velocity in the channel along the axial flow direction for smooth channel and channel with VG, with and without gravity. The results show the regions where the flow is normal ($0 \leq X/D \ll 25$), disrupted due to VG installation ($X/D = 25$) and recovering ($25 \leq X/D \ll 275$). In the normal flow region, the velocity experiences gradual increase of the same magnitude for all curves, whereas in the disrupted region, the velocity rises very rapidly and drops just after the VG. In the recovering region, the velocities for the smooth channel and channel with VG without gravity almost completely overlap whereas when gravity is considered, there exist sections of distinguishable velocity declines due to major and minor HTDs. More specifically, the velocity declines are more severe for smooth channel under gravity and occur earlier than those of the channel with VG. Thus, it can be concluded that VG inclusion in the flow channel weakens the buoyancy effect on the turbulent heat transfer thereby suppressing and delaying HTD upon flow recovery.

5. Annular channel simulation

5.1. Grid convergence test

Grid independent test was conducted for the annular channels with and without VGs as shown in **Fig. 18**. For both scenarios, the axes of 2D computational domains are set as x and r . The grid size along the axial z -direction is 2 mm and uniform. In the radial r -direction, the grids near the wall were refined so that y^+ of the first grid near the wall is less than 1 and the first grid node can be located in the viscous sublayer. Hence, non-uniform grids were employed in r -direction. The size of the first element near the wall is 0.001 mm and the ratio is 1.08. The grid number increases from 34,000 to 66,000 elements and simulation results show that wall temperature no longer changes when the grid number is 47,000. For the annular channel with VGs, further mesh refinement was carried out and it was found that channel with VG requires more grid numbers to attain convergence and capture its effects more accurately. The VG of height 0.2 mm is arbitrarily selected for grid convergence test. The results indicate that the wall temperature no longer changes significantly when the grid number for the channel with VG is greater than 60,000.

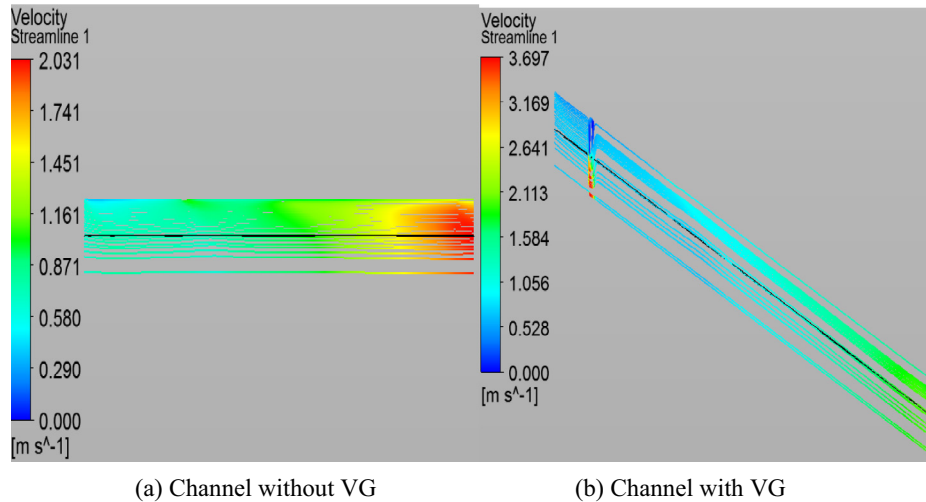


Fig. 13. Comparison of velocity streamlines in a circular channels.

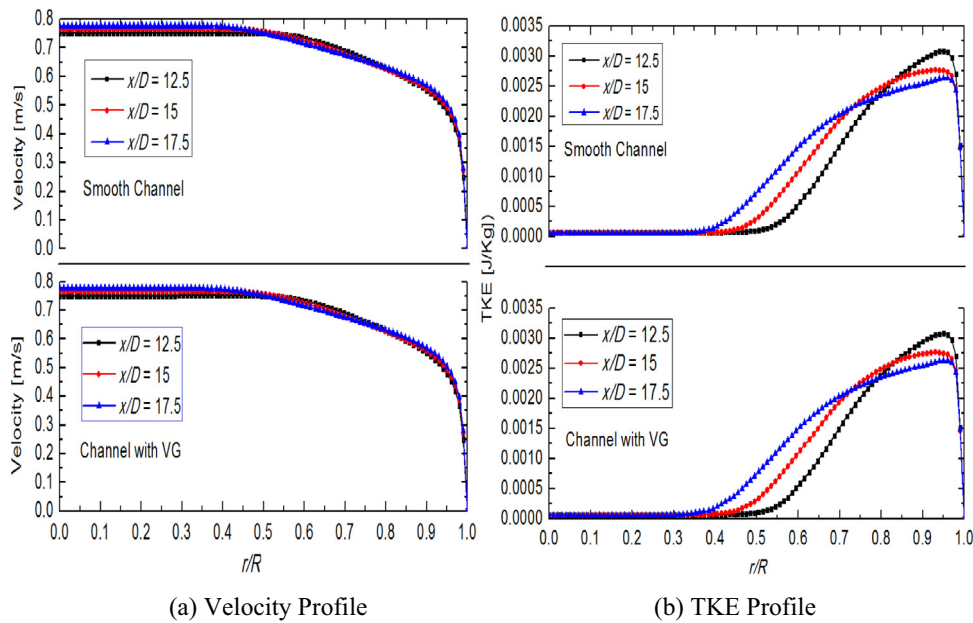


Fig. 14. Velocity and TKE distributions at different axial positions of Phase 1 before VG.

6. Annular channel results and discussions

6.1. Wall temperature distribution in the annular channel without VGs

The axial temperature distribution when no VG is installed in the annular channel is shown in Fig. 19. It can be seen that at such high heat flux and low mass flux, wall temperature increases drastically and reaches a peak of 679 °C at an axial position, $x = 210$ mm. This is the so-called HTD phenomenon. Since such high temperature may cause the failure of the fuel rod and even core meltdown in SCWR, hence by mitigating the temperature peaks when HTD occurs via VG installation, the probability of core meltdown can be significantly reduced.

6.2. Effect of size

The effect of different sizes of VGs on the HTD is shown in Fig. 20. Fig. 20(a) that the temperature peaks are nearly the same,

which means that the size of VGs has little effect on the mitigation of HTD in this channel. The HTC and its normalised form are presented in Fig. 20 (b) and Fig. 20 (c) respectively. It is seen that, just as in the circular channel, HTC also shows a couple of oscillations downstream of the VGs. However, these oscillations damp out earlier (at $x/D = 75$) when compared with those of circular channel (at $x/D = 180$), hence minimising greatly the HTD delay effects of VGs in annular channel. This phenomenon can be explained that the size of the VG and the length scale are much smaller in annular channel than the case of circular channel, and the area affected by the vortices induced by VG is therefore very limited. Hence, VG only causes the mixing of the main flow and boundary layer flow locally and has little effect on the bulk flow.

Fig. 21 illustrates the radial velocity and TKE distributions at different axial positions in the downstream of the VG. The axial position where the VG is installed is at $x = 150$ mm ($x/D = 18.75$). It can be seen from **Fig. 21** (a) that at the axial position nearest the VG end ($x/D = 20$), the velocity near the wall increases significantly.

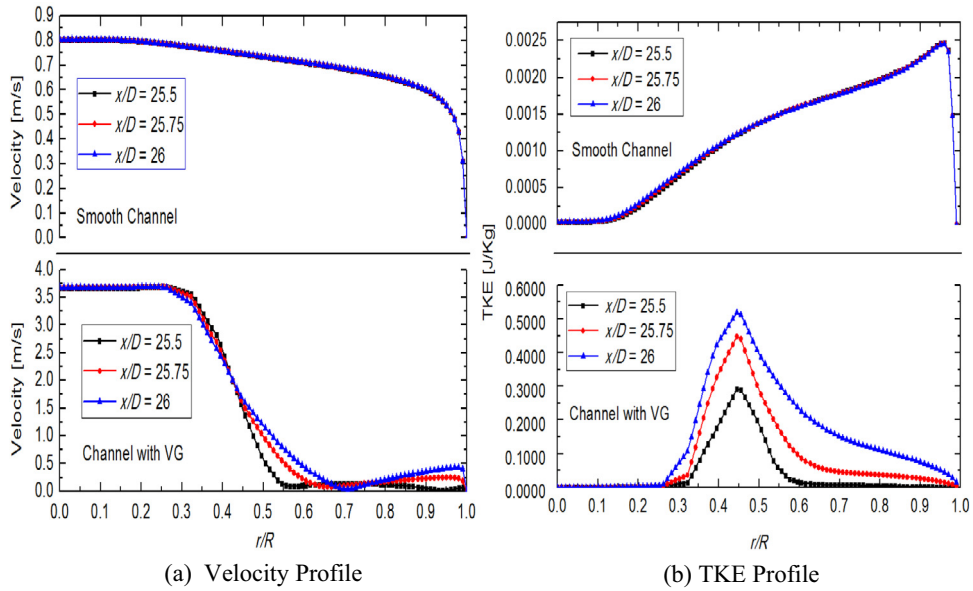


Fig. 15. Velocity and TKE distributions at different axial positions of Phase 2 in VG downstream.

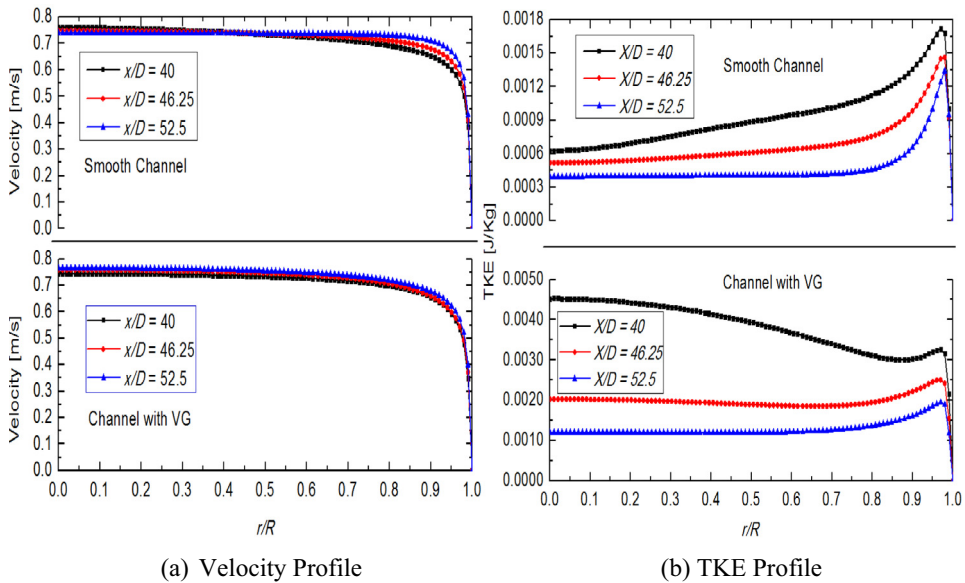


Fig. 16. Velocity and TKE distributions at different axial positions of Phase 3 in VG downstream.

cantly. Here, the sudden area flow reduction around the VGs causes a strong secondary flow in the radial direction. Near the outer wall as shown in Fig. 21(b), the TKE also increases significantly leading to an increase in heat transfer performance. It could also be seen that the near-wall velocity profile is flattened and leads to suppression of TKE in the near-wall region at $x/D = 22.5\text{--}27.5$. Hence, wall temperature increases drastically again and reaches its peak, but this peak is lower and a little bit moved downstream compared with smooth channel.

6.3. Position effect

Wall temperature variations in the annular channel when VGs are placed at different axial positions are shown in Fig. 22. Similar to the circular channel, significant suppression, and delay of HTD are observed when VG is placed close to the point where HTD occurs, whereas when it is placed further away before this position

this effect greatly reduces. Also, in order to avoid placing a VG at points where HTD already occurs, the start of the major HTD baseline ($x = 150$ mm) is taken to be the highest position where VG is placed. At this position, the temperature peak drops by about 47 °C.

6.4. Effect of number

The wall temperature distribution with different number of VGs each placed at the start of major peak baseline are shown in Fig. 23. It can be seen that the highest peak with one, two and three VGs are 632 °C, 562 °C, and 520 °C respectively. So peak temperature only drops by 47 °C with one VG, while it drops by as high as 117 °C with two VGs and 159 °C with three VGs when compared with No VG case. Hence, like the circular channel, increasing the number of VGs increases its suppression and delay effects on HTD with pressure drop penalty.

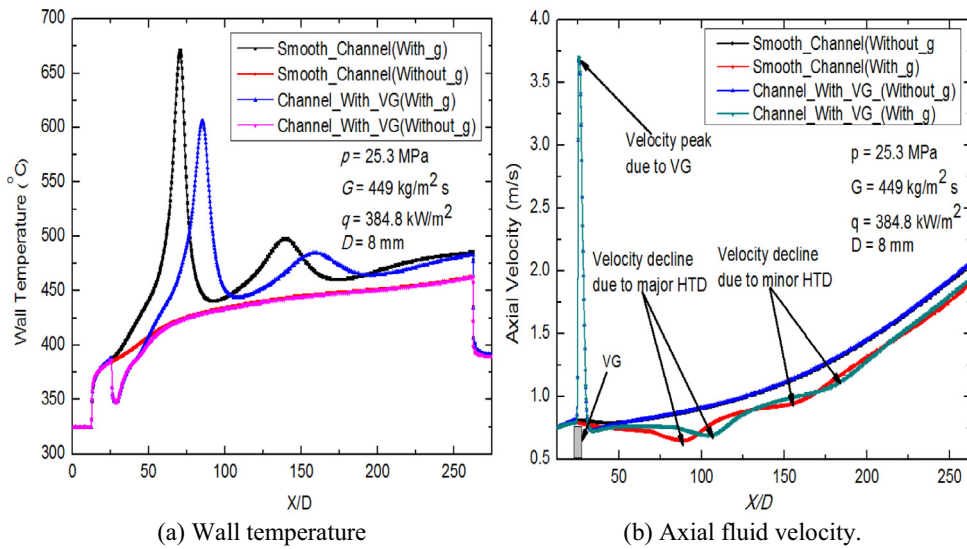


Fig. 17. Further investigation of effects of VG on buoyancy flow.

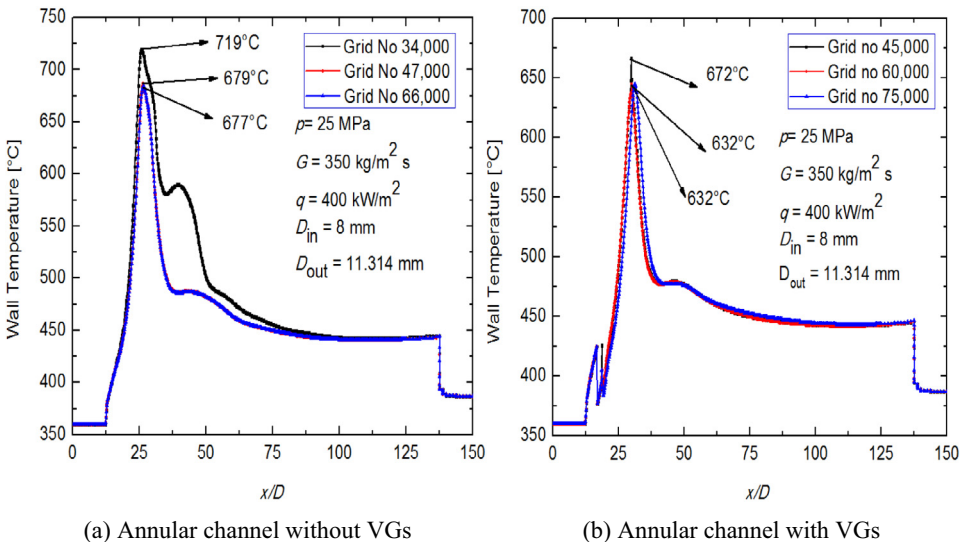


Fig. 18. Grid independence tests.

7. Total pressure losses

The use of VGs in thermal hydraulics comes with higher pressure drop penalty, Δp . The total pressure drop was measured in FLUENT by the difference between the pressure at inlet and outlet of the test section based on the mass-weighted total pressure loss. The presence of the fully developed flow at the entrance of the heated section and absence of reverse flow in the outlet section makes this classical approach suitable to evaluate overall pressure losses [39]. The pressure drop relative difference for each VG case studied is the percentage difference relative to the smooth case in each channel. The total pressure drop for smooth circular and annular channels are 1473 Pa and 1601 Pa respectively. The total pressure drops and the corresponding relative difference due to the size, position and number of VGs in both channels are shown in Table 3 and Table 4 respectively. For both channels, the bigger the size and number of VGs, the higher the pressure drop. It is worth noting that the values of the total pressure drop due to optimal sized VGs for circular and annular channels are 1580 Pa and 1729 Pa respectively. Except for the total pressure drops for circular channel VGs of sizes (3.0 mm by 2.0 mm) and (3.5 mm by

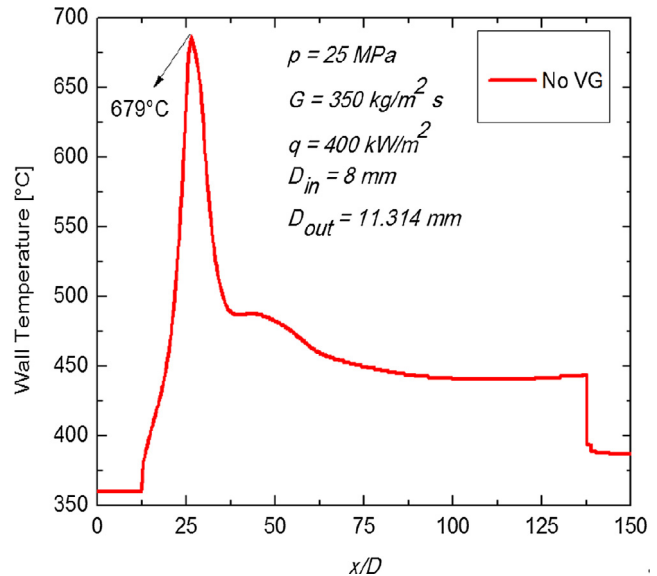


Fig. 19. Annular channel axial wall temperature distributions.

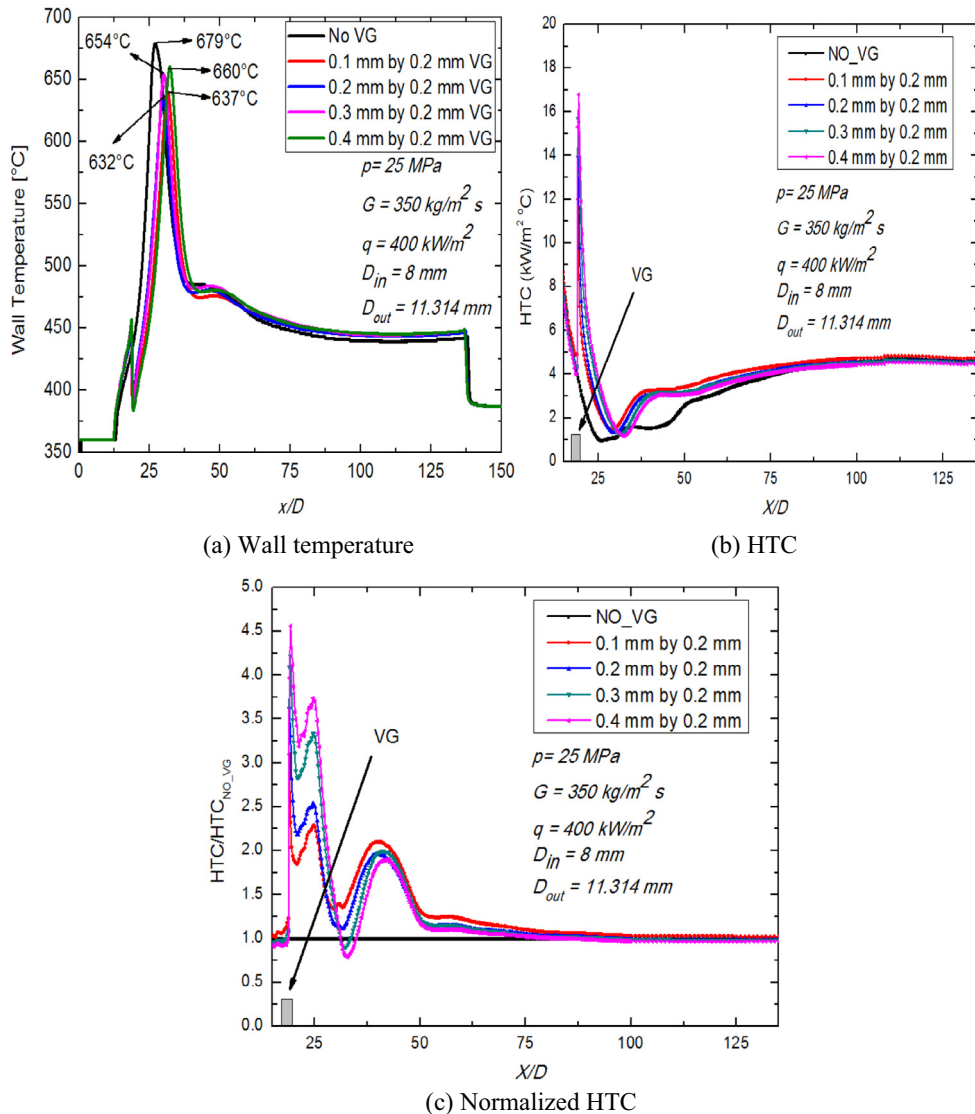


Fig. 20. Effects of VGs size on HTD in annular channel.

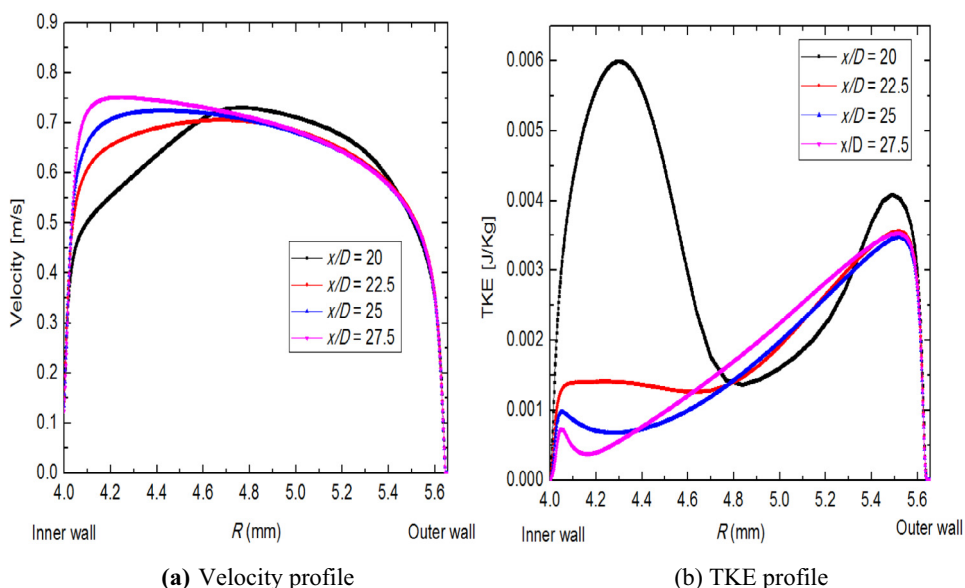


Fig. 21. Velocity and TKE distributions at different axial positions in annular channel downstream of VG.

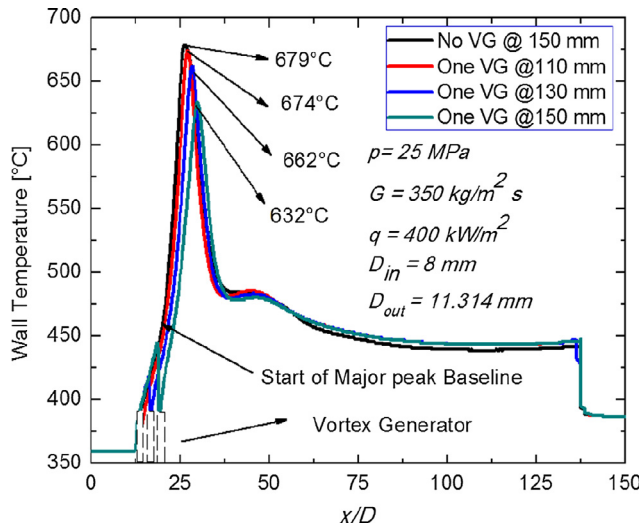


Fig. 22. Effects of Positions of VG on HTD in the annular channel.

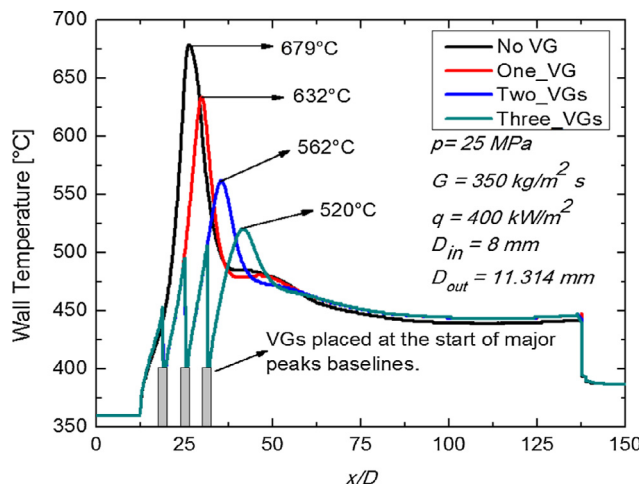


Fig. 23. Annular channel axial wall temperature distribution with different number of VG.

Table 4
Pressure drop for Annular Channel with VGs.

Case	Total Pressure drop, Δp (Pa)	Δp rel. diff., %
Smooth channel	1601	reference case
1-Size (H (mm) by L (mm))		
(i)	1615	0.9
(ii)	1729	8.0
(iii)	1895	18.4
(iv)	2500	56.2
2-Position (mm)		
(i)	1695	5.9
(ii)	1701	6.3
(iii)	1729	8.0
3-Number		
(i)	1729	8.0
(ii)	1850	15.6
(iii)	2001	25.0

2.0 mm) whose values are relatively high, others are very small and can be ignored when compared with the supercritical water pressure. So in our design to mitigate HTD, the VGs have little effect on the main flow.

8. Conclusions

In this paper, the effects of vortex generators on heat transfer deterioration is numerically studied for supercritical water flowing upward in circular and annular channels at high heat flux and low mass flux using SST $k-\omega$ turbulence model in ANSYS-FLUENT. The effects of VG's size, position, and number on HTD are investigated, and based on these, the following conclusions are summarized:

The results show that the size, position and number of VGs have suppression and delay effects on HTD downstream of the VGs. There exists optimal size of VG which can have a suppression effect on HTD, and beyond which this effect starts to diminish. The VG's position has the most significant effect on HTD for any single VG. At the locations where VGs are installed, and at the downstream locations, strong effect of VG on HTC is observed, with the normalized HTC showing that the wall temperature oscillates a couple of times before becoming stable when the flow returns to fully developed state. Mechanism analysis based on the radial distributions of velocity and TKE at different axial positions reveals that HTD suppression is caused by the weakening of the buoyancy effect due to increased TKE near the wall downstream of the VG whereas the delay is caused by the boundary layer recovery effect due to flow redevelopment after being disrupted by the VG.

9. Declaration of conflicting interests

The author(s) hereby declare no potential conflicts of interest with respect to the research, authorship and/or publication of this article.

Acknowledgments

This work is partially supported by The Science Technology and Innovation Committee of Shenzhen Municipality through project number: JCYJ20150601102053068.

Appendix A. Supplementary material

Supplementary data to this article can be found online at <https://doi.org/10.1016/j.ijheatmasstransfer.2019.03.145>.

References

- [1] U. Kashyap, K. Das, B.K. Debnath, Effect of surface modification of a rectangular vortex generator on heat transfer rate from a surface to fluid, *Int. J. Therm. Sci.* 127 (2018) 61–78.
- [2] Y.L. He, Y. Zhang, Advances and outlooks of heat transfer enhancement by longitudinal vortex generators, in: *Advances in Heat Transfer*, Elsevier, 2012, pp. 119–185.
- [3] A.M. Jacobi, R.K. Shah, Heat transfer surface enhancement through the use of longitudinal vortices: a review of recent progress, *Exp. Therm. Fluid Sci.* 11 (3) (1995) 295–309.
- [4] M. Fiebig, Vortices, generators and heat transfer, *Chem. Eng. Res. Des.* 76 (2) (1998) 108–123.
- [5] S. Sripathanapipat, P. Promvonge, Numerical analysis of laminar heat transfer in a channel with diamond-shaped baffles, *Int. Commun. Heat Mass Transf.* 36 (1) (2009) 32–38.
- [6] M. Awais, A.A. Bhuiyan, Heat transfer enhancement using different types of vortex generators (VGs): a review on experimental and numerical activities, *Therm. Sci. Eng. Prog.* (2018).
- [7] S.Y. Yoo, D.S. Park, M.H. Chung, S.Y. Lee, Heat transfer enhancement for fin-tube heat exchanger using vortex generators, *KSME Int. J.* 16 (1) (2002) 109–115.
- [8] S. Caliskan, Experimental investigation of heat transfer in a channel with new winglet-type vortex generators, *Int. J. Heat Mass Transf.* 78 (2014) 604–614.
- [9] C. Wang, L. Luo, L. Wang, B. Sundén, Effects of vortex generators on the jet impingement heat transfer at different cross-flow Reynolds numbers, *Int. J. Heat Mass Transf.* 96 (2016) 278–286.
- [10] G. Lu, G. Zhou, Numerical simulation on performances of plane and curved winglet-Pair vortex generators in a rectangular channel and field synergy analysis, *Int. J. Therm. Sci.* 109 (2016) 323–333.

- [11] K.W. Song, S. Liu, L.B. Wang, Interaction of counter rotating longitudinal vortices and the effect on fluid flow and heat transfer, *Int. J. Heat Mass Transf.* 93 (2016) 349–360.
- [12] I. Pioro, S. Mokry, Thermophysical properties at critical and supercritical pressures, *Heat Transfer-Theoretical Analysis, Experimental Investigations and Industrial Systems*, InTech, 2011.
- [13] M.E. Shitsman, Impairment of the heat transmission at supercritical pressures (Heat transfer process examined during forced motion of water at supercritical pressures), *High Temp.* 1 (1963) 237–244.
- [14] A.P. Ornatskiy, L.F. Glushchenko, O.F. Gandzyuk, An experimental study of heat transfer in externally-heated annuli at supercritical pressures, *Heat Transfer-Sov. Res* 4 (1972) 25.
- [15] J.D. Jackson, K. Evans-Lutterodt, Impairment of turbulent forced convection heat transfer to supercritical pressure CO₂ caused by buoyancy forces, *Res. Report NE* 2 (1968).
- [16] W.B. Hall, J.D. Jackson, Laminarization of a Turbulent Pipe Flow by Buoyancy Forces, ASME paper. no 69-HT-55, 1969.
- [17] W.B. Hall, J.D. Jackson, Heat transfer near the critical point, in: *Advances in Heat Transfer*, Elsevier, 1971, pp. 1–86.
- [18] J.D. Jackson, M.A. Cotton, B.P. Axcell, Studies of mixed convection in vertical tubes, *Int. J. Heat Fluid Flow* 10 (1) (1989) 2–15.
- [19] J.D. Jackson, Fluid flow and convective heat transfer to fluids at supercritical pressure, *Nucl. Eng. Des.* 264 (2013) 24–40.
- [20] J. Wang, J. Li, J.D. Jackson, A study of the influence of buoyancy on turbulent flow in a vertical plane passage, *Int. J. Heat Fluid Flow* 25 (3) (2004) 420–430.
- [21] H.Y. Gu, Z.X. Hu, D. Liu, H.B. Li, M. Zhao, X. Cheng, Experimental study on heat transfer to supercritical water in 2×2 rod bundle with wire wraps, *Exp. Therm. Fluid Sci.* 70 (2016) 17–28.
- [22] Y.Y. Bae, H.Y. Kim, T.H. Yoo, Effect of a helical wire on mixed convection heat transfer to carbon dioxide in a vertical circular tube at supercritical pressures, *Int. J. Heat Fluid Flow* 32 (1) (2011) 340–351.
- [23] X. Zhu, S. Morooka, Y. Oka, Numerical investigation of grid spacer effect on heat transfer of supercritical water flows in a tight rod bundle, *Int. J. Therm. Sci.* 76 (2014) 245–257.
- [24] Y. Xiao, J. Pan, H. Gu, Numerical investigation of spacer effects on heat transfer of supercritical fluid flow in an annular channel, *Int. J. Heat Mass Transf.* 121 (2018) 343–353.
- [25] Han Wang, Qincheng Bi, Zhendong Yang, Wu Gang, Hu Richa, Experimental and numerical study on the enhanced effect of spiral spacer to heat transfer of supercritical pressure water in vertical annular channels, *Appl. Therm. Eng.* 48 (2012) 436–445.
- [26] Zhen-xiao Hu, Han-yang Gu, Heat transfer of supercritical water in annuli with spacers, *Int. J. Heat Mass Transf.* 120 (2018) 411–421.
- [27] Yan Guo, Gu Chenglong, Wei Tian, Weicai Li, Analysis on the dynamic buckling behavior of the spacer grid structure pp. V003T02A048-V003T02A048, 2018 26th International Conference on Nuclear Engineering, American Society of Mechanical Engineers, 2018.
- [28] C.F.M. Schettino, J.P. Gouveia, N. Medeiros, Analyses of spacer grids compression strength and fuel assemblies structural behavior, *Nucl. Eng. Des.* 260 (2013) 93–103.
- [29] D. Palko, H. Anglart, Theoretical and numerical study of heat transfer deterioration in high performance light water reactor, *Sci. Technol. Nucl. Install.* 2008 (2008).
- [30] M. Jaromin, H. Anglart, A numerical study of heat transfer to supercritical water flowing upward in vertical tubes under normal and deteriorated conditions, *Nucl. Eng. Des.* 264 (2013) 61–70.
- [31] H. Cheng, J. Zhao, M.K. Rowinski, Study on two wall temperature peaks of supercritical fluid mixed convective heat transfer in circular tubes, *Int. J. Heat Mass Transf.* 113 (2017) 257–267.
- [32] E.W. Lemmon, M.L. Huber, M.O. McLinden, *NIST Standard Reference Database 23: Reference Fluid Thermodynamic and Transport Properties-REFPROP*, Version 9.1, National Institute of Standards and Technology, Standard Reference Data Program, Gaithersburg, 2013.
- [33] X. Cheng, B. Kuang, Y.H. Yang, Numerical analysis of heat transfer in supercritical water cooled flow channels, *Nucl. Eng. Des.* 237 (3) (2007) 240–252.
- [34] J. Yang, Y. Oka, Y. Ishiwatari, J. Liu, J. Yoo, Numerical investigation of heat transfer in upward flows of supercritical water in circular tubes and tight fuel rod bundles, *Nucl. Eng. Des.* 237 (4) (2007) 420–430.
- [35] I.B. Celik, U. Ghia, P.J. Roache, Procedure for estimation and reporting of uncertainty due to discretization in [CFD] applications, *J. Fluids [Engineering-Transactions] (ASME)* 130 (7) (2008).
- [36] K. Podila, Y. Rao, Computational fluid dynamic simulations of heat transfer from a 2×2 wire-wrapped fuel rod bundle to supercritical pressure water, *J. Nucl. Eng. Radiat. Sci.* 4 (1) (2018) 011008.
- [37] A. Kiss, A. Churkin, D.S. Pilkhwal, A.M. Vaidya, W. Ambrosini, A. Pucciarelli, K. Podila, et al., Summary on the results of two computational fluid dynamic benchmarks of tube and different channel geometries, *J. Nucl. Eng. Radiat. Sci.* 4 (1) (2018) 011001.
- [38] Q. Zhang, H. Li, X. Lei, J. Zhang, X. Kong, Study on identification method of heat transfer deterioration of supercritical fluids in vertically heated tubes, *Int. J. Heat Mass Transf.* 127 (2018) 674–686.
- [39] D. Lengani, D. Simoni, M. Ubaldi, P. Zunino, F. Bertini, Turbulent boundary layer separation control and loss evaluation of low profile vortex generators, *Exp. Therm. Fluid Sci.* 35 (8) (2011) 1505–1513.